

## Mechanical Properties of WC-12Co HVOF Coatings

M. Jalali Azizpour<sup>1</sup> S. Norouzi<sup>2</sup>, H. Mohammadi Majd<sup>3</sup>

<sup>1,3</sup> Department of Mechanical Engineering, Ahwaz branch, Islamic Azad University, Ahwaz, Iran

<sup>2</sup>Babol University of Technology, Babol, Iran

[Mahdi.jalali.azizpour@gmail.com](mailto:Mahdi.jalali.azizpour@gmail.com)

**Abstract:** In this paper, Agglomerated WC-12 Co powder was coated on AISI1045 steel using high velocity oxy fuel (HVOF) method and its microstructure, residual stress, bonding strength and fatigue behaviour were evaluated. The results have shown that the developed coating has more than 64.55 MPa adhesive strength and 156-257 MPa compressive residual stresses. The S-N curves of the coated and un-coated samples revealed a good agreement. Morphological and crystallographical studies were conducted using optical microscopy, scanning electron microscopy (SEM) and X-ray diffraction respectively to evaluate the powder and coating characteristics.

[M. Jalali Azizpour, S. Norouzi, H. Mohammadi Majd. Mechanical Properties of WC-12Co HVOF Coatings. Journal of American Science 2011; 7(9):609-614]. (ISSN: 1545-1003). <http://www.americanscience.org>. 79. doi:[10.7537/marsjas070911.79](https://doi.org/10.7537/marsjas070911.79)

**Keywords**—HVOF, Residual stress, WC-12Co, Fatigue

### 1. Introduction

Thermal spray is a promising method replacing the hazardous chrome plating in the finishing industry. This method has demonstrated to have superior wear and fatigue properties when compared to hard chromium using cermets e.g. tungsten carbide-cobalt (WC-Co). High velocity oxy fuel (HVOF) coatings have exhibited wear resistant WC-Co coating with high density; superior bond strength and less decarburization than many other thermal spray methods. This is attributed to its high particle impact velocities and relative low peak particle temperature [1],[2]. The main challenge remains on control of residual stress imposed primarily by quenching (fast cooling from melting point to substrate temperature) which is of tensile nature and secondary by the difference in the thermal expansion coefficients between the coating ( $\alpha_c$ ) and substrate ( $\alpha_s$ ), which leads to residual stresses induced by the mismatch of thermal shrinkage during cooling from the process temperature to room temperature, during the so called secondary cooling]. The high velocity impact of semimolten particles on the substrate in the HVOF spray process is revealed as peening stress which is of compressive nature. The final total residual stress through the whole coating/substrate system which directly affects its bonding strength is the sum of the above mentioned stresses together with the compressive stress state of the substrate induced during the grit blasting prior to spraying [3]. One of the concerns in thermal spray process is determining the residual stress. The level of this stress and its sign has a significant effect on coating performance. A number of techniques have been used in the past decades to measure residual stresses in thermal spray coatings. Curvature measurement methods rely on the

monitoring of changes in component distortion, either during deposition or after. Diffraction methods are based on the elastic deformations within a polycrystalline material to measure internal stresses in coatings. The stresses cause deformation i.e., changes in the distance between the lattices, which are used as internal strain gages. Shifts in diffraction peaks are recorded from which the strain distribution is calculated. Diffraction methods are based on the elastic deformations within a polycrystalline material to measure internal stresses in coatings. The stresses cause deformation i.e., changes in the distance between the lattices, which are used as internal strain gages. Shifts in diffraction peaks are recorded from which the strain distribution is calculated [2], [3].

In this study mechanical property of coating in high speed gas compressor shafts (up to 23000 rpm) using high velocity oxy fuel thermal spray method has been investigated. This coating was developed based on pre-studied standard experiments (fatigue, bond strength, and residual stress); Morphological and crystallographical studies were conducted using optical microscopy, scanning electron microscopy (SEM) and X-ray diffraction respectively to evaluate the powder and coating characteristics.

### 2. Material and Methods

AISI 1045 steel substrate samples were industrially coated using HVOF gun (Metjet III, Metallization). Before deposition, substrate was grit blasted with SiC particles (16 $\mu$ m mesh) and ultrasonically cleaned in acetone. The WC-12Co particle size was between 15-40 $\mu$ m. The spray parameters are according to Table 1. The remained parameters were indicated by the company. In the as deposited condition, the coating had an average roughness of  $\sim$ 4  $\mu$ m. Residual stress

evaluation by curvature and X-ray diffraction coupled by removal method was investigated on 120x20x1.5 mm<sup>3</sup> 20x10x3 mm samples respectively. The static mechanical properties of the investigated materials were evaluated by means of tensile testing employing a computer controlled servo hydraulic machine. The results are given in table2. Furthermore fatigue and bonding strength evaluations were conducted on samples prepared according to ASTM E466 and ASTM C633 respectively. The samples were evaluated in as spray condition. The microhardness indentation procedure used is given in the relevant ASTM E384-10 Standard. Through thickness microhardness profile obtained from the Vickers hardness machine in 2.94N load. The average coating porosity also has been considered. The porosity analysis was determined by optical image analysis.

Table1: Thermal spraying parameters

Fuel rate (l/min)	250
Oxygen rate (l/min)	830
Spray distance (mm)	340± 10
Spray angle (deg)	90

Table2: Mechanical properties of substrate

Ultimate Tensile Stress	547 MPa
Yield Stress	278.5 MPa
Elongation	18.21 %

### 3. Results and discussion

XRD, SEM, image analysis were performed to evaluate the crystalline structure phases, morphological and porous structure of the WC-12Co powder and its coating respectively.

#### 3.1 Crystallographic characterization

Fig.2 illustrates the XRD pattern of WC-12Co powder. As it can be seen from the patterns the peaks are attributed to WC and Co. Figure 3 illustrates the XRD pattern of the coating. As it can be seen the patterns correspond to presence of WC, W<sub>2</sub>C and W<sub>6</sub>Co<sub>6</sub>C. The presence of W<sub>2</sub>C and W<sub>6</sub>Co<sub>6</sub>C are thought to be due to decomposition of WC at high temperature of flame jet and abundant amount of oxygen when the powders are accelerated. Decarburisation of WC has been reported in the literature to affect the coating hardness and wear resistance [2]. In the work of Stewart et al. [4], it has been established that the formation of W<sub>2</sub>C upon splat quenching is caused by dissolution of WC in Co matrix whereas the formation of elementary W

depended on the composition of the starting powder. Yang et al. [5] showed that larger degree of WC decomposition is correlated to a smaller carbide grain size in the starting powder. Other forms of W-Co-C may also be present in the matrix in the form of W<sub>x</sub>Co<sub>y</sub>C<sub>z</sub> which are not detected by the XRD method due to their low content or high dispersion in the coating.

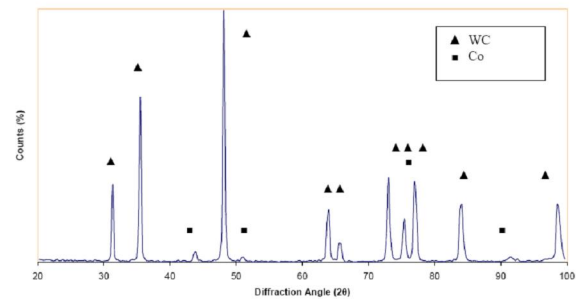


Fig.1: XRD pattern of WC-12Co powder

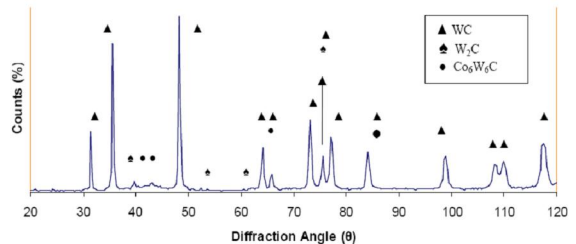


Fig.2: XRD pattern of WC-12Co coating

#### 3.2 Morphological characterization

Fig. 3 illustrates the Scanning Electron Microscopy (SEM) morphology of agglomerated WC-12Co powder in 500x magnification. As observed the particles are spherical and uniformly distributed (15-45 μm) with high porosity.

Fig.4 shows the SEM topography of the coating at the free surface. As illustrated the coating has an agglomerated morphology consisting of WC-Co. The agglomerates can be clearly seen. The microstructure consists of a network of WC-Co agglomerates. WC-Co agglomerates are formed where WC particles are dispersed in Co matrix resulting in high peripheral porosity as a result of WC particle moving towards the centre of agglomerates. This can be clearly observed in the micrograph. The porosity is thought to be intrinsic phenomena in thermal spray coating because of process nature which must be limited by controlling the process parameters. Fig. 5 illustrates a general view of the coating after metallographic preparation. The WC-12Co HVOF thermally sprayed coating appear to be quiet dense. The porosity analysis determined by optical microscopy and image analysis shows apparent porosity less than 1%. The presence of lamella boundaries, pores and well

distribution of WC grains of different size embedded in the Co matrix is apparent.

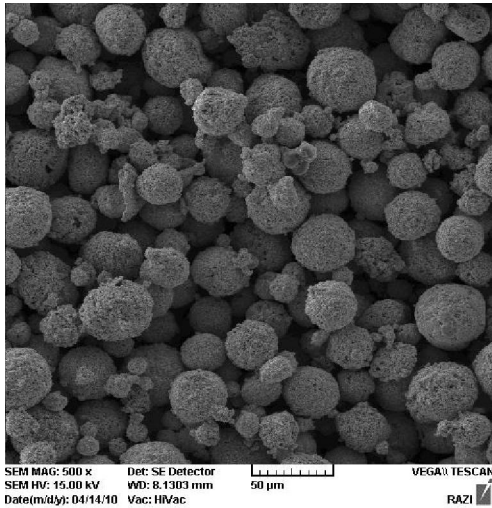


Fig.3: Particle morphology in 500x magnification

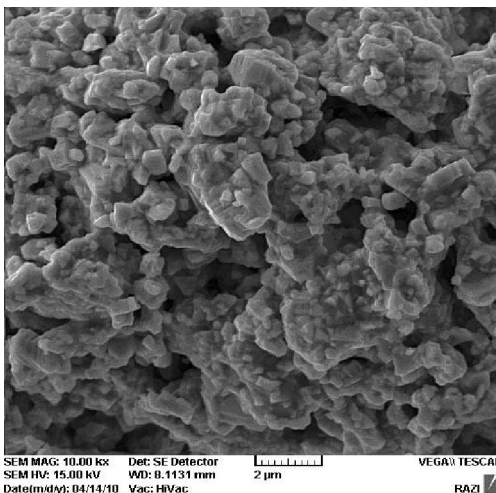


Fig.4: SEM topography coating surface

### 3.3 Microhardness characterization

The measuring is done using an eyepiece micrometer. Hardness is calculated according to the following formula:

$$HV = \frac{F(Kgf)}{A(mm^2)} = \frac{2F \sin(\alpha/2)}{d^2} \times 1000$$

$$= 1854 \frac{F}{d^2}$$

where  $F$  is the test load and  $A$  is surface area of indentation. The angle between faces on the Vickers' diamond is  $136^\circ$ .

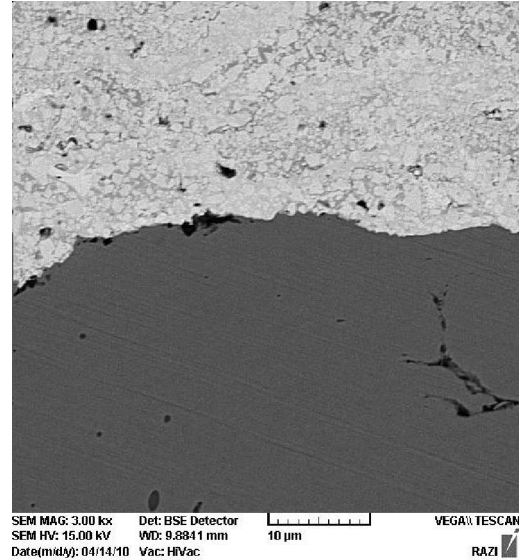


Fig.5: SEM micrograph of substrate-coating interface

As it can be seen in Fig.6 the hardness is not uniform through the coating thickness and in 0.3 mm the hardness is in maximum value (1397HV). For this cemented carbide thermal spray coating, the average of measured hardness numbers was 1166 HV. The wear resistance of thermally sprayed WC-12Co coating is attributed to be due to high hardness of these coatings.

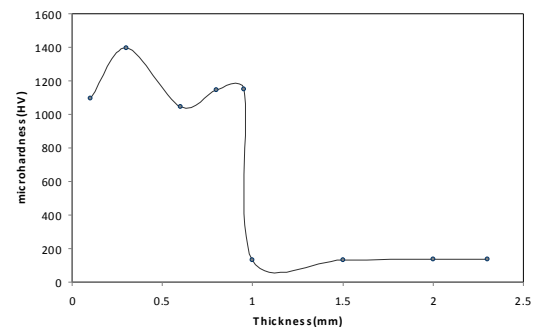


Fig.6: Microhardness profile of coating

### 3.4 Residual stress

#### 3.4.1 Curvature method

The Stony equation [6] is used to obtain the relationship the residual stress and the curvature [7]:

$$\sigma_r = -\frac{kE_s t_s^2}{6(1-\nu_s)t_c}$$

Which the  $k$  ( $=1/R$ ) represent the final curvature,  $t_s$  substrate thickness,  $t_c$  coating thickness.  $E_s$  and  $\nu_s$  are the elastic modulus and Poisson ratio of substrate respectively. Residual stress evaluation was performed using post-mortem curvature method on appropriate samples. Stony's equation was used for this purpose. Three different thicknesses was thermally sprayed on the AISI 1045 steels samples

(350±20 μm, 650±20 μm and 980±20 μm). The curvature of coated strip was measured by using Coordinate Measurement Machine (CMM). Stony's equation parameters are given in table3. The Superposition of residual stresses with tensile and compression natures are evaluated to be compressive. The mean value estimated for residual stress is presented in Fig.7. As it can be seen from the results, as the thickness is increased the compressive residual stress is reduced.

Table3: Stony's equation parameters in this study

Sample	R(m)	E <sub>s</sub> (GPa)	v <sub>s</sub>	t <sub>c</sub> (mm)	t <sub>s</sub> (mm)
1	1250	210	0.3	0.35	1.5
2	915	210	0.3	0.65	1.5
3	735	210	0.3	0.98	1.5

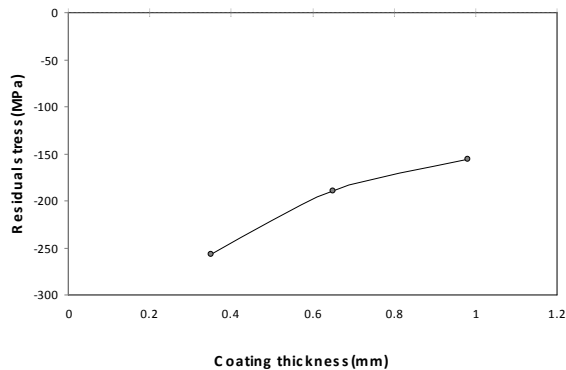


Fig.7: Compressive Residual stress from curvature method

### 3.4.2 XRD method

In XRD method the measurement relies on the stresses in polycrystalline structure. The position of the diffraction peak undergoes shifting as the specimen is rotated by an angle  $\psi$ . The magnitude of the shift is related to the magnitude of the residual stress. The relationship between the peak shift and the residual stress ( $\sigma$ ) is given [3]:

$$\sigma = \frac{E}{(1+\nu)\sin^2\psi} \frac{(d_n - d_i)}{d_i}$$

where E is Young's modulus,  $\nu$  is Poisson's ratio,  $\psi$  is the tilt angle, and  $d_i$  is the d spacing measured at each tilt angle. If there are no shear strains present in the specimen, the d spacing changes linearly with  $\sin^2\psi$ . The residual stresses were determined by means of X-ray diffraction employing a diffractometer and using Cu-K $\alpha$  radiation. Electropolishing was employed for layer removal. The residual stress estimation was done in a  $\psi$ -geometry. The strain in the samples were measured using the (201) reflection of WC for peak position ( $2\theta=78.22$ ), the values of penetration depth were around  $\sim 2\mu\text{m}$  with X-ray

absorption coefficient determined according to [2], [8]. The average through thickness residual stress measured to be  $-190\pm 50$  MPa revealing the compressive nature of stresses. This is in good agreement with the results of Y.Y Santana reporting  $-179$  MPa and  $-220$  MPa through thickness using hole drilling method and XRD (201 reflection) respectively [2]. These compressive stresses are thought to be due to peening effects as a result of high velocity and impact of the WC-Co particles upon coating process. The analysis results emphasized the significance of peening stress in controlling the final stress state of the coated specimen due to high velocity and kinetic Energy during the HVOF spraying process. The effects of residual stress on the mechanical properties of the coating namely compressive residual stress could significantly improve the coating properties, where the tensile stress impaired the coating property [9], [10].

### 3.5 Adhesion test

The bonding samples were machined; sand blasted, ultrasonically cleaned, thermally sprayed and tested according to ASTM633-03. The studies have shown that in all of the samples the failure was from binder suggesting the adhesive strength of binder used is less than the bonding strength of WC-Co deposited by high velocity oxy fuel (a limitation). The results show that the failures occurred at 56.86, 60.94, 54.82, 64.55, 61.37 MPa respectively, clearly revealing that the adhesive and cohesive strength of the coating is greater than 64.55 MPa. It is to note that this evaluation method assumed that the interface stress was uniform; it was based on the concept of average interface stress or nominal stress. As a result, it can't reflect the true interface strength characteristic because of the stress singularity near the interface. Bonding between particles and substrates is critical to ensure the quality of coating. In this study spherical particles have been used. The spherical particles (see Fig.3) require less kinetic energy for good adhesion on the substrate as mentioned previously in the literatures [11].

### 3.6 Fatigue test

Samples were prepared according to ASTM E466 with  $350\pm 50$  μm coating. The rotation-bending test was conducted with respect to uncoated substrates. The rotation-bending test was made by SANTAM fatigue machine. The evaluation of the static mechanical properties indicated that the uncoated substrate has a yield stress of 284 MPa and ultimate tensile of 540 MPa (Table2). These properties were not modified significantly due to grit blasting and coating as mentioned previously in the literatures

[12-14]. The S-N curve of coated and uncoated AISI 1045 illustrated in Fig.8 The results indicate a good agreement in the trend for the coated and un-coated samples, however the fatigue limit of coated samples was  $\sigma_e=0.43\sigma_u$  which is less than the fatigue limit of uncoated samples ( $\sigma_e=0.46\sigma_u$ ). The decrease in fatigue strength for the coated substrates can be attributed essentially to the superposition of the compressive residual stress induced by the HVOF thermal spray and effect of grit blasting process, as mentioned previously in the literatures [12-16].

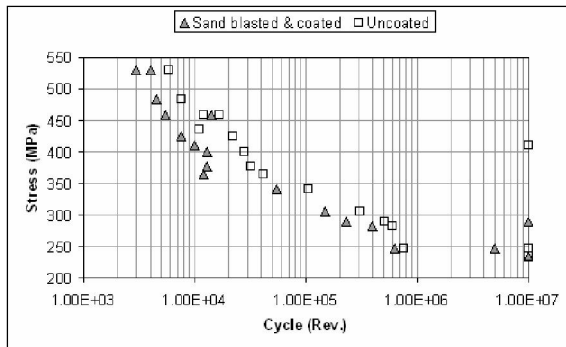


Fig.8: S-N curves for coated and uncoated AISI1045

Fig.9 illustrates the fatigue cracks in the coating normal to interface. The normal cracks are presumed to be primarily initiated from the surface. The cracks can initiate from porosity, a shot peen cavity or any other pre-treatment reasons. Coating failure occurs when such cracks propagate and link together in the interface. Fig.10 clearly shows the initiation and propagation of crack at the interface in the work hardened substrate and debonding of coating from the substrate

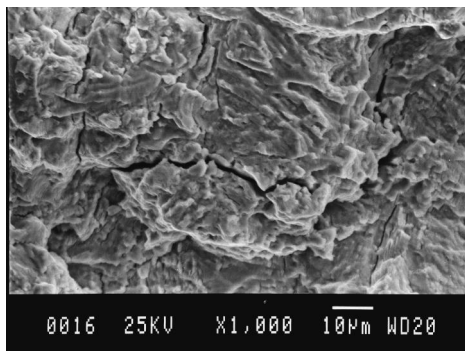


Fig.9: SEM micrograph of cracks in the coating

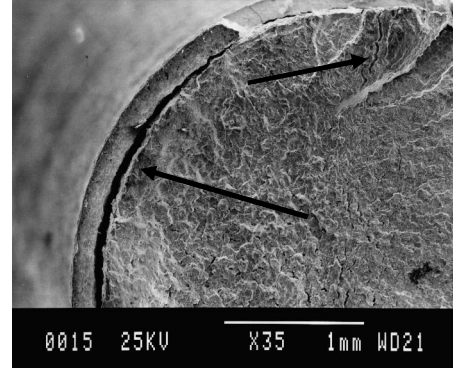


Fig.10:SEM micrograph of crack and fatigue failure

#### 4. Conclusion

Mechanical property of coated high speed shafts using high velocity oxy fuel thermally spraying process has been investigated. Metallurgical and mechanical investigations were employed for this purpose. A summary of conclusions is as follow:

- The residual stress in coating with 0.35 mm thickness is estimated to be -257MPa by curvature method and  $-190\pm 50$  MPa by X-ray diffraction method.
- WC-12Co cermet coating has bonding strength more than 64.55 MPa but developing a new approach – binder independent- for testing of adhesive and cohesive strength is an important necessity.
- Compressive residual stresses improve the fatigue behavior coated parts but preparation process could affect the fatigue life of these parts in their service.
- the fatigue limit of coated samples was  $\sigma_e=0.43\sigma_u$  which is less than the fatigue limit of uncoated samples ( $\sigma_e=0.46\sigma_u$ )

#### Acknowledgment

The authors gratefully acknowledge the financial support provided by the Islamic Azad University Ahwaz branch and technical support by the R&D section of PACO (Powderafshan, Isfahan, Iran)

#### Corresponding Author:

Mehdi Jalali Azizpour  
Department of Mechanics  
Islamic Azad University, Ahwaz branch  
Ahwaz, Iran  
E-mail: [mjalali@iauhvaz.ac.ir](mailto:mjalali@iauhvaz.ac.ir)

**References:**

1. M. HeydarzadehSohi, F.Ghadami, Comparative tribological study of air plasma sprayed WC–12%Co coating versus conventional hard chromium electrodeposit, *Tribology International*, 2009.
2. Y.Y. Santana, Characterization and residual stresses of WC–Co thermally sprayed coatings, *Surface & Coatings Technology* 202 (2008) 4560–4565
3. C. Lyphout, Residual Stresses Distribution through Thick HVOF Sprayed Inconel 718 Coatings, *Journal of Thermal Spray Technology*, Volume 17(5-6) Mid-December 2008—915.
4. Stewart DA, Shipway PH, McCartney DG. Microstructural evolution in thermally sprayed WC–Co coatings *Acta Mater* 2000;48:1593–604.
5. Yang Q, Senda T, Ohmori A. Effect of carbide grain size on microstructure and sliding wear behavior of HVOF-sprayed WC–12% Co coatings. *Wear* 2003;254:23–34.
6. T.C. Totemeier, R.N. Wright, W.D. Swank, *Metall. Mater. Trans., A Phys. Metall. Mater. Sci.* 35 (6) (2004) 1807.
7. T.C. Totemeier, R.N. Wright, *Surf. Coat. Technol.* 200 (12-13) (2006) 3955.
8. J.C. Smithells, *Metals Reference Book*, 5th edition Butterworths, London, 1976.
9. T.C. Totemeier, Residual stress determination in thermally sprayed coatings—a comparison of curvature models and X-ray techniques, *Surface & Coatings Technology* 200 (2006) 3955 – 3962.
10. R.T.R. McGrann, The effect of coating residual stress on the fatigue life of thermal spraycoated steel and aluminum, *Surface and Coatings Technology* 108–109 (1998) 59–64
11. S. Kamnis, Numerical modeling the bonding mechanism of HVOF sprayed particles, *Computational Materials Science* 46 (2009) 1038–1043.
12. E.S. Puchi-Cabrera, M.H. Staia, Fatigue behavior of a SAE 1045 steel coated with Colmonoy 88 alloy deposited by HVOF thermal spray, *Surface & Coatings Technology*, 2010
13. M.Y.P. Costa, M.L.R. Venditti, H.J.C. Voorwald, M.O.H. Cioffi, T.G. Cruz, Effect of WC–10%Co–4%Cr coating on the Ti–6Al–4V alloy fatigue strength, *Materials Science and Engineering A* 507 (2009) 29–36
14. S. Watanabe, Fatigue Cracks in HVOF Thermally Sprayed WC-Co Coatings, *Journal of Thermal Spray Technology*, Volume 7(1) March 1998-93.
15. R.T.R. McGrann, D.J. Greving, J.R. Shadley, E.F. Rybicki, B.E. Bodger, and D.A. Somerville, The Effect of Residual Stress in HVOF Tungsten Carbide Coatings on the Fatigue Life in Bending of Thermal Spray Coated Aluminum, *Journal of Thermal Spray Technology*, 546---Volume 7(4) December 1998.
16. S. Fouvry, K. Kubiak, Introduction of a fretting-fatigue mapping concept: Development of a dual crack nucleation – crack propagation approach to formalize fretting-fatigue damage, *International Journal of Fatigue*, 31 (2009) 250–262.

8/9/2011